Development of a Compact and Efficient Liquid Cooling System With Silicon Microcooler for High-Power Microelectronic Devices

Gongyue Tang, Yong Han, Boon Long Lau, Xiaowu Zhang, *Senior Member, IEEE*, and Daniel Min Woo Rhee

***Abstract*— In this paper, a compact and efficient single-phase liquid cooling system is developed for the microelectronic devices with high-power dissipation, such as the high performance servers, power amplifiers, and airborne systems. The developed system includes three major components: 1) a silicon-based hybrid microcooler; 2) a customized compact liquid-to-liquid heat exchanger; and 3) a commercial micropump. Our focus in this paper is on the efficiency improvement for the full cooling system, which includes the development of the silicon-based hybrid microcooler, and the optimization of the miniaturized heat exchanger with low pressure drop, small footprint area, and high heat exchange efficiency. The following accomplishments have been obtained through this paper. The developed microcooler combines the merits of both microjet array impingement and microchannel flow cooling technologies. The optimized heat exchanger is with about 50% of pressure drop, nearly 10% of the footprint area, and around 420% of heat transfer density of a commercial heat exchanger investigated in this paper as a benchmark. The developed system has been demonstrated with the heat dissipation capability of 350 W/cm^2 on a chip of 7 mm × 7 mm (a total power of 175 W) with a low pumping power of 0.1 W.**

***Index Terms*— Compact heat exchanger, liquid cooling system, microchannel, microjet array impingement, single-phase, thermal management.**

I. Introduction

THE increasing demand for enhanced functionality, higher reliability, smaller form factor, and lower cost in electronic devices has led to the development of large-scale integrations and miniaturizations. These large-scale integrations and miniaturizations in turn cause the steady increase in the power dissipation from the electronic chips and systems. Therefore, advanced cooling technology is required and it has attracted the attention of many researchers. For example, Madhour *et al.* [1] offer a parametric study with single- and two-phase cooling technologies to address the cooling requirements for the future vertically integrated microprocessors. Mizuno *et al.* [2] develop a silicon microchannel cooler-based thermal management device for the high-power amplifiers. Mohapatra and Loikits [3] provide a study on what attributes are more effective in selecting a working fluid for a microchannel application. Wei and Joshi [4] offer a thermal resistance modeling approach to show the potential beneficial and deleterious effects associated with stacking microchannels. In general, air cooling can provide a simple, low cost, effective, and reliable cooling solution. However, with the increase in heat flux dissipation, the air-cooling technology is not sufficient anymore. According to Suszko [5], the upper limit of the power dissipation heat flux for dedicated air-cooling solutions is 50 W/cm^2. When the heat flux goes beyond 100 W/cm^2, air-cooling methods have become inadequate for most applications [6], [7]. Such liquid cooling technology for microelectronic devices with high-power chips is required. Previously, a number of researchers have explored the advantages of using liquid cooling to mitigate the presented thermal management problems [8]–[12]. Basically, there are two major modes of liquid cooling technology, such as single-phase cooling and two-phase cooling. Considering the higher pressure drop and more complexity of a two-phase liquid cooling system, utilizing the single-phase liquid cooling technology for high-heat-flux microprocessors is a viable option [13], [14]. For a single-phase liquid cooling technology, both microchannel and microjet heat sinks can dissipate high heat fluxes anticipated in high-power electronic devices [15]–[17]. Robinson [18] compared the performance of microchannel cooling and microjet array impingement cooling for high-power application in detail, and much higher peak heat transfer coefficient was obtained from the microjet array impingement cooling than that from the microchannel cooling. In addition, Brunschwiler *et al.* [19] demonstrated that a microjet array impinging cooling method can provide a high heat transfer coefficient up to 8.7×10^4 W/m^{2}K. Compared with the impinging microjets, microchannel cooling has a lower averaged heat transfer coefficient but the coolant in microchannels can exchange energy with a larger effective surface area with multiple walls within each of the channels. Li and Peterson [20] conducted a detailed numerical simulation of the heat transfer occurring in silicon-based microchannel heat sinks to optimize the geometric structure. The effect of the microchannel geometry on the temperature distribution in the microchannel heat sink is presented and discussed, assuming a constant pumping power [20]. Colgan *et al.* [21] described a practical implementation of a single-phase silicon microchannel cooler designed for cooling very high-power

Manuscript received September 25, 2015; revised February 26, 2016; accepted March 13, 2016. Date of publication April 6, 2016; date of current version May 13, 2016. This study is supported by the Silicon Micro Cooler (SMC) consortium project, and the consortium members include Honeywell Aerospace and Element Six Technologies. Recommended for publication by Associate Editor S. H. Bhavnani upon evaluation of reviewers' comments.

The authors are with the Institute of Microelectronics, Agency for Science, Technology and Research, Singapore 117685 (e-mail: tangg@ime.a-star.edu.sg; hany@ime.a-star.edu.sg; laubl@ime.a-star.edu.sg; xiaowu@ime.a-star.edu.sg; rheem@ime.a-star.edu.sg).

Color versions of one or more of the figures in this paper are available online at http://ieeexplore.ieee.org.

Digital Object Identifier 10.1109/TCPMT.2016.2542848

chips, and the cooler of this design was able to cool a single chip with the average power densities of 300 W/cm^2 by bonding this chip to the cooler using the silver epoxy or solder. Recently, the hybrid microcooler, combining the merits of both microjet array impingement and microchannel flow, has been applied for cooling the high-power devices [22], [23].

All of the above studies are focused on the development of the microcooler with an embedded microchannels/microjet array to maximize their heat dissipation capability. The thermal design for the external heat exchanger is not well addressed. However, the heat exchanger could be a limiting factor in the application scenarios, such as data center and airborne systems, where both weight and size become of a practical concern. Miniaturized heat exchanger with low pressure drop and high heat exchange efficiency is a major design concern for cooling system designers. Available studies on a single miniaturized heat exchanger are reported in [24] and [25], which, nonetheless, did not consider the hydraulic performance and thermal efficiency of a full system, including the microcooler for integrated circuits (ICs) cooling.

In this paper, an efficient and compact single-phase liquid cooling system is proposed and developed. The proposed liquid cooling system includes three major components: 1) a silicon-based hybrid microcooler with multiple drainage microtrenches (MDMTs); 2) a customized compact liquid-to-liquid heat exchanger; and 3) a commercial micropump. The design target for this cooling system is with heat dissipation capability of 350 W/cm^2 on a chip of 7 mm $\times$ 7 mm (a total power of 175 W). Such a liquid cooling system is targeted to the applications of the high-performance servers for datacenters, airborne systems, and the power amplifiers. In order to achieve such a high performance, the following efforts have been made in this paper: 1) develop a silicon-based hybrid microcooler, combining the merits of both microjet array impingement and microchannel flow cooling technologies and 2) optimize a compact and efficient heat exchanger with low pressure drop, small form factor, and high heat exchange efficiency.

II. System Design and Fabrication

A compact liquid cooling system for a microelectronic chip is shown in Fig. 1(a). It mainly consists of a microcooler to remove the heat from the high performance chip, a commercial micropump to drive the liquid flow, and the liquid flow transport the heat from the chip to an external heat exchanger, where the heat is transferred to the secondary fluid and then rejected to the ambient. There are two liquid flow loops in this cooling system, as shown in Fig. 1(b); the first one is the flow loop at the chip cooling side (i.e., hot flow loop) and the other is the flow loop at the thermostat side (i.e., cold flow loop). For the heat flow, the heat flux is first transferred from the thermal chip to the microcooler, then transported to the heat exchanger, and at last rejected to the ambient through the thermal bath equipment, as shown in Fig. 1(c).

To maximize the performance of the system, the following design criteria should be considered in the design of the proposed liquid cooling system [26].

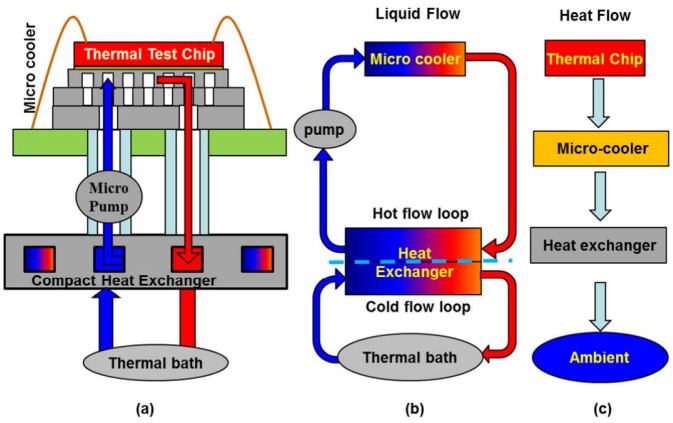

Fig. 1. Schematic of the compact liquid cooling system. (a) Concept design of the system. (b) Liquid flow loops in the system. (c) Heat flow path in the system.

1) To avoid large pressure drop and also to minimize the negative consequence in case of aqueous liquid leakage, which is detrimental to the electronic components, the flow rate in the loop at chip cooling side should be maintained at a low level.
2) The heat exchanger should have compact size with high heat exchange efficiency, or heat transfer density as termed in this paper. Reduction in size and weight but with the same or similar performance has been one of the key design considerations.
3) It is required to maintain the thermal resistance and pressure drop of the heat exchanger at a level obviously lower than that of the microcooler. This is to reduce the design burden for the chip cooling design and unnecessary cost due to chip cooling assembly requirement.

A. Hybrid Silicon-Based Microcooler

A silicon-based microcooler, combining the merits of both microchannels and jet impingement, has been developed to dissipate the heat flux for the high-power IC chip. MDMTs have been designed inside the cooler to avoid the negative cross-flow effect between the nearby nozzles [21]. Fig. 2 shows the conceptual design of the hybrid silicon microcooler for the pattern of the microchannels, jet nozzles, and MDMTs, the side view of the *A–A* cross section, which illustrates the flow paths from the jet nozzle to the microchannels and then to MDMTs, the 3-D isometric view, which shows the microchannels, jet nozzles, and MDMTs, and *C–C* view, which shows the cross section of the microchannels.

As shown in Fig. 2(a), there are two nozzles between each of the two trenches in our proposed MDMTs design. The jet flow from the microjet nozzle impinges on the top wall, is constrained to flow along the microchannel, and then exits through the nearby drainage microtrenches [see Fig. 2(b)]. As elaborated and explained in the previous works [22], there will be no cumulative accumulation of the cross flow to cause detrimental influence on the adjacent jet impingement with this MDMTs configuration. Therefore, the fully developed impingement can be achieved for all individual nozzles, which will enable more uniform and higher cooling capability for the chip.

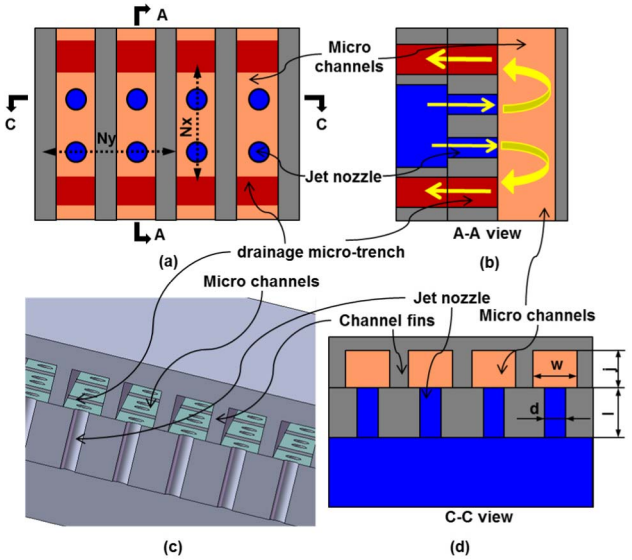

Fig. 2. Schematic of the proposed hybrid microcooler with MDMTs design. (a) Pattern of the microchannels, jet nozzles, and MDMTs. (b) Side view of the *A*–*A* cross section. (c) 3-D isometric view. (d) *C*–*C* cross-sectional view.

In this paper, the computational fluid dynamics (CFD)-based modeling and simulation is conducted using FLOTHERM for the microcooler design optimization. For the chip of size 7×7 mm^2, the microjet array is designed to cover an area of 8×8 mm^2 for the cooling. Considering the fabrication capability and process maturity, the jet nozzle diameter (d) is fixed at 100 μm. The nozzle length (l), microchannel width (w), and jet to wall (JTW) distance (j) are varied in the modeling to evaluate their effects on the thermal performance of the microcooler. Other parameters for the simulation are listed as the followings. Nine drainage trenches with a width of 150 μm are configured in the microcooler. The number of the nozzles along the microchannel direction (Nx) is 16 (with a pitch of 250 μm within two trenches and 550 μm cross the trenches). The number of the jet nozzles along the drainage trench direction (Ny) is 21 (with a pitch of 350 μm). The coolant in the microcooler is water with an inlet temperature of 25 °C. Heat source of 175 W is set for the thermal chip, and a gauge pressure of 20 kPa is set at inlet of the microcooler. A mesh of 1 million is generated, and the grid independence study is conducted. The mesh number is sufficient to obtain accuracy within around 1% for hydraulic and thermal performance.

The effects of the nozzle length, microchannel width, and JTW distance on the thermal performance of the microcooler are, respectively, presented in Figs. 3–5. Fig. 3 shows that the junction to microcooler thermal resistance increases as the jet nozzle length increases. This is because the pressure loss in the jet nozzle increases as the jet nozzle length increases, as such weaken the jet performance. However, it can be found from Fig. 3 that the increment of thermal resistance is negligible when the jet nozzle length varies from 300 to 600 μm. Fig. 4 shows that the thermal resistance decreases when the microchannel width increases from 150 to 250 μm, while the thermal resistance increases again as the microchannel width increases further to 300 μm. This can be attributed to the

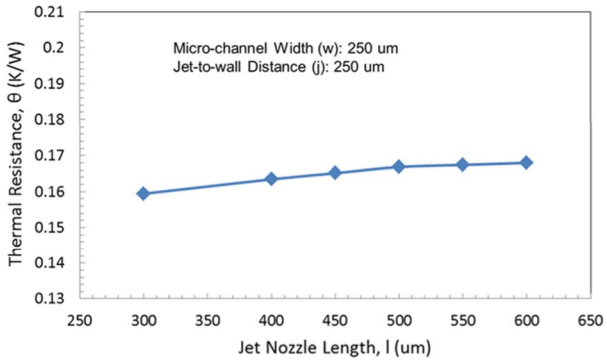

Fig. 3. Variation of junction to microcooler thermal resistance with jet nozzle length.

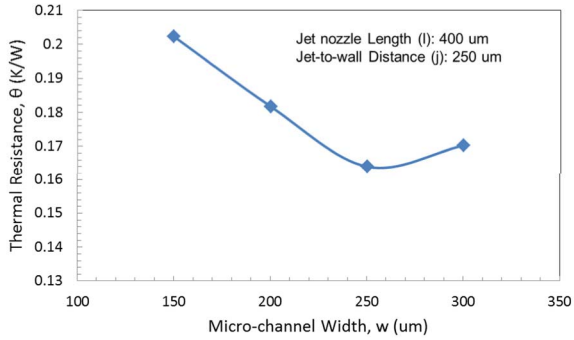

Fig. 4. Variation of junction to microcooler thermal resistance with microchannel width.

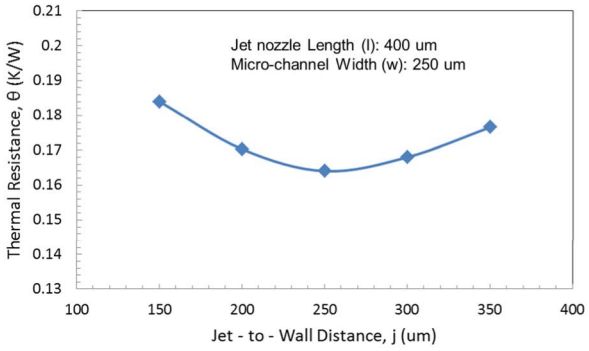

Fig. 5. Variation of junction to microcooler thermal resistance with JTW distance.

reduction of heat conduction capability through the thinned microchannel fins with an increase in microchannel width. Fig. 5 shows that the optimal thermal performance can be achieved when the JTW distance is 250 μm for the proposed microcooler. Based on above analysis, the microcooler with a jet nozzle diameter of 100 μm, a nozzle length of 400 μm, a JTW distance of 250 μm, and a microchannel width of 250 μm will be fabricated for the experimental study.

The hybrid microcooler is fabricated by bonding two major patterned silicon layers together, as shown in Fig. 6. The first layer consists of the patterned microchannels and fins. The second layer is a double side patterned layer, which consists of the jet nozzles/MDMTs on one side and inlet flow arrangement trenches and MDMT outlets on the other side.

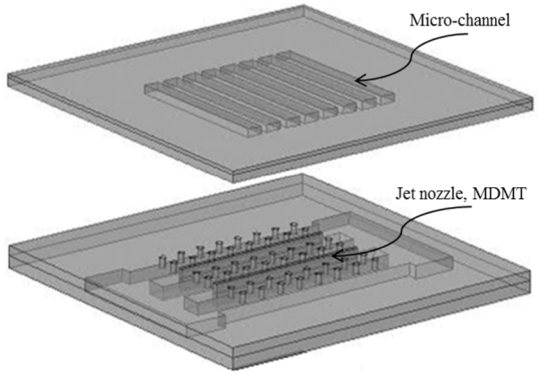

Fig. 6. Exploded view of the proposed silicon microcooler (the material is set to be transparent for illustrating the internal details of the cooler).

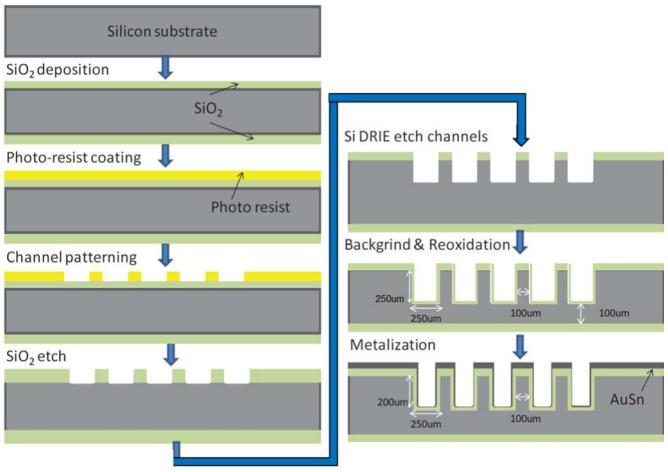

Fig. 7. Fabrication process flow of the microchannel with DRIE technology.

The microchannels and fins, microjet nozzle arrays, MDMTs, flow arrangement trenches, inlets, and outlets of the microcooler are fabricated by using the deep reactive ion etching (DRIE) process technology. As an example for the DRIE process technology, the fabrication process for a microchannel layer is shown in Fig. 7. It starts with a blank 8-in wafer. First, a layer of SiO_2 with a 3-μm thick is deposited by plasma-enhanced chemical vapor deposition (PECVD) process in a Novellus PECVD system, and then the SiO2 layer is patterned and etched as hard mask with microchannel patterns. The microchannels are further etched using the DRIE process to reach a depth of 250 μm. After that, the back side of the wafer is grinded to 350-μm thickness. At last, stacked metal layers of Ti 1000 A, Pt 2000 A, Au 2 μm, Sn 2 μm, and Au 500 A are deposited for the chip-level AuSn eutectic bonding later. The inlets and outlets in the intermedia layer are fabricated using the similar process flow. The microjet nozzles/drainage trenches and flow arrangement layer is also fabricated on the doubles sides of the wafer using DRIE technology, please refer to [27] for details.

After all the features are formed in the separate wafer, the wafer is then diced into chip level and continues the subsequent chip-level bonding and packaging process. The image of the each fabricated layer is shown in Fig. 8 for a microchannel layer, and the microjet nozzle and flow arrangement layer.

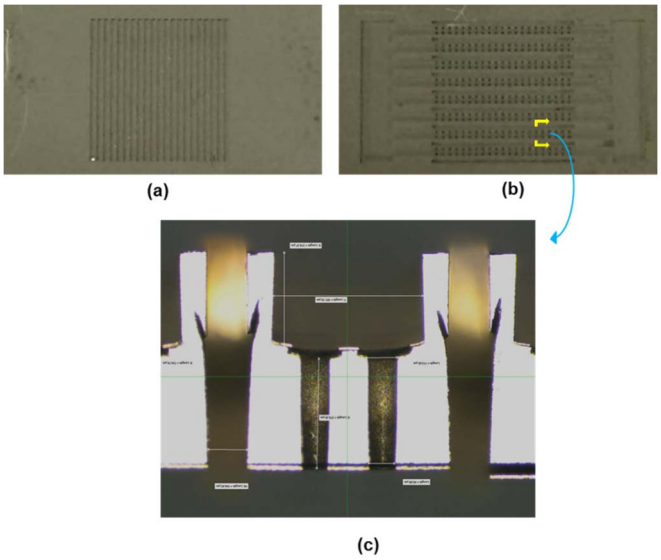

Fig. 8. Fabricated components of the microcooler. (a) Image of the microchannel layer. (b) Image of the microjet and flow arrangement layer. (c) Microscopy images of the cross section details of the microjet and flow arrangement trenches.

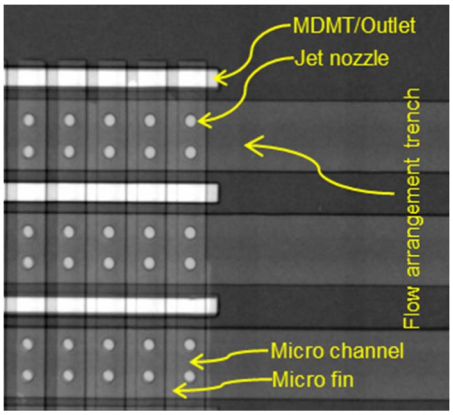

Fig. 9. X-ray image of the assembled microcooler (after TCB bonding process).

The cross section details of the microjet nozzle/MDMT and flow arrangement trenches are shown in Fig. 8(c).

After the wafer is diced into chips, the chip-level bonding is conducted to bond the microchannel layer and the microjet/MDMT layer together. The bonding is carried out through the thermal compression bonding (TCB) process, in which the 280 °C chuck holding time is 2 min and the compressive force is 49 N. Fig. 9 shows the X-ray image of the assembled microcooler. Following the microcooler fabrication, the top surfaces of the microcooler are metalized for the thermal test chip to microcooler attachment. As last, the thermal test chip is bonded to the top surface of the microcooler by using the same TCB process. The fabricated microcooler has been conducted a dedicated leakage test at a gauge pressure of 60 kPa and no leakage is observed.

B. Heat Exchanger

A conventional fin-tube heat exchanger requires fans to remove the heat from extended fins around the cooling tube. Such configuration could be oversized in space constrained

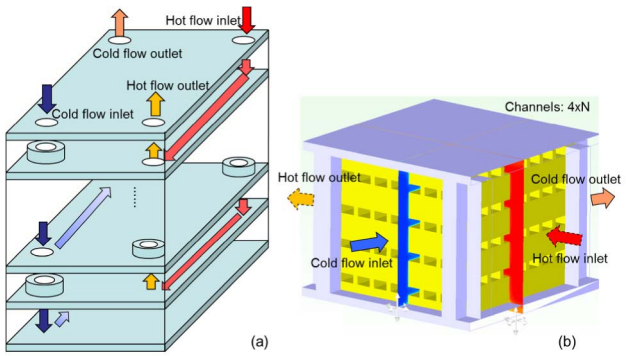

Fig. 10. Schematic configurations of the heat exchangers investigated in this paper for (a) counter-flow configuration of commercial heat exchanger A (Hex-A) and (b) cross-flow configuration of customized heat exchanger B (Hex-B).

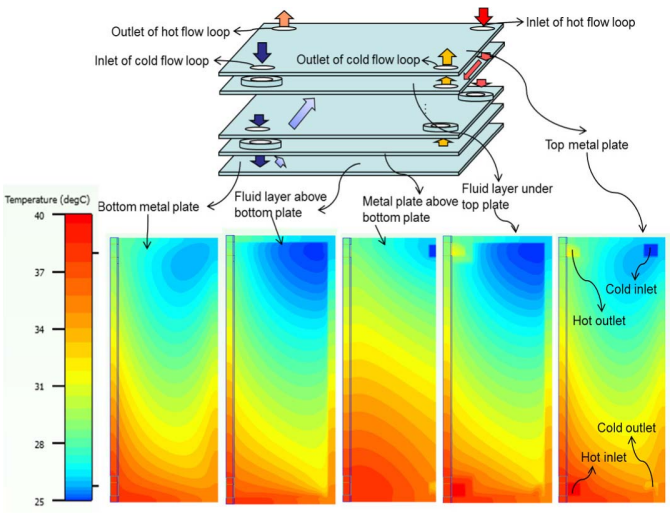

Fig. 11. Simulation results of the temperature profiles in the commercial heat exchanger A.

electronic systems, and the noncentralized air flow would also overheat the peripheral electronic parts, accompanied with other design limitations, such as fan noise. Instead, a liquid to liquid heat exchanger has the advantage of higher heat exchange efficiency, smaller size, and centralized management of the secondary liquid flow through facility cooling, such as coolant distributed unit.

Two liquid-to-liquid heat exchanger configurations are investigated in the present case. The first heat exchanger (Hex-A) is commercially available with counter-flow configuration, and it is used as a benchmark to design and optimize the second heat exchanger (Hex-B). Hex-B is a customized compact heat exchanger, which represents the cross-flow configuration, consisting of mini-channel layers alternatively stacked for both the hot and cold fluid flows. Hex-A is with the counter-flow configuration, as shown in Fig. 10(a); the hot fluid and cold fluid layers are stacked alternatively, separated with metal plates. There are totally 11 stainless steel (SS) layers, including the top and bottom cover plates with a thickness of 1.1 mm for each layer. These metal layers form ten layers of liquid channels, which include five layers for the cold liquid and five layers for the hot liquid. Bonding of the different metal layers is done through brazing tooling and process at vendor's site to form the heat exchanger without fluid leakage; the overall size of Hex-A is with a length of 204 mm, a width of 74 mm, and a height of 25 mm. Hex-B is designed with cross-flow configuration, as shown in Fig. 10(b), in which the hot fluid and cold fluids are stacked, with the two types of flow channels arranged at an angle of 90°, to form the heat exchanger. Hex-B is targeted to have similar performance as Hex-A while have smaller footprint size than that of the Hex-A.

CFD-based software (i.e., FLOTHERM) is utilized to simulate the thermal and flow profiles in the heat exchangers. In this paper, the inlet flow rate is varied from 0.4 to 2 L/min with a fixed temperature of 25 °C for the cold flow loop of the heat exchangers, whereas the flow rate is fixed to 0.4 L/min for the hot flow loop. The inlet flow temperature in the hot flow loop of the heat exchanger is fixed to 40 °C for case study. Due to the relatively small Reynolds number, the laminar flow is assumed in this paper. A mesh of 530 K is generated and the grid independence study is conducted. The mesh number is sufficient to obtain accuracy within around 1% for hydraulic and thermal performance.

The fields of flow, pressure, and temperature are obtained through the modeling and simulation; as such the liquid temperature at different locations can be captured through the obtained temperature profiles. The performance of commercial Hex-A is used to benchmark the performance of optimized Hex-B. Fig. 11 shows the simulation results of the temperature profile in Hex-A. In this case, the flow rate is 0.4 L/min in both the cold flow loop and the hot flow loop; the inlet fluid temperature is of 25 °C in cold flow loop and 40 °C in the hot flow loop of the heat exchanger.

With the temperature profiles obtained through the modeling and simulations (i.e., Fig. 11 for Hex-A and Fig. 15 for Hex-B), the amount of heat transferred by the heat exchanger can be derived from the difference of enthalpy for either the hot fluid or cold fluid, namely

$$Q = E_{h\text{in}} - E_{h\text{out}} \tag{1a}$$

or

$$Q = E_{c\text{out}} - E_{c\text{in}} \tag{1b}$$

where Q is the amount of heat transferred by the heat exchanger (W). $E_{h\text{in}}$ and $E_{h\text{out}}$ are the inlet and outlet fluid enthalpy in the hot flow loop of the heat exchanger (W), respectively. $E_{c\text{in}}$ and $E_{c\text{out}}$ are the inlet and outlet fluid enthalpy in the cold flow loop of the heat exchanger (W), respectively.

Furthermore, the heat transfer density, which refers to the amount of heat per unit volume transferred by the heat exchanger (i.e., Q over the volume of the heat exchanger), is extracted to evaluate the thermal effectiveness of the heat exchangers involved in this paper. The variation of the heat transfer density with liquid flow rate for Hex-A is shown in Fig. 12. In this case, the flow rate in the hot flow loop is fixed at 0.4 L/min. The inlet fluid temperature is 25 °C for the

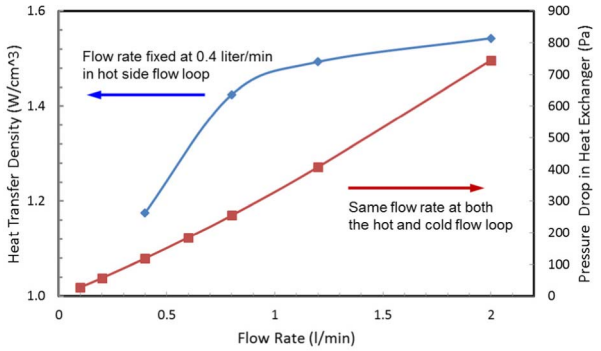

Fig. 12. Variation of the heat transfer density and pressure drop with the flow rate in Hex-A at the specified conditions.

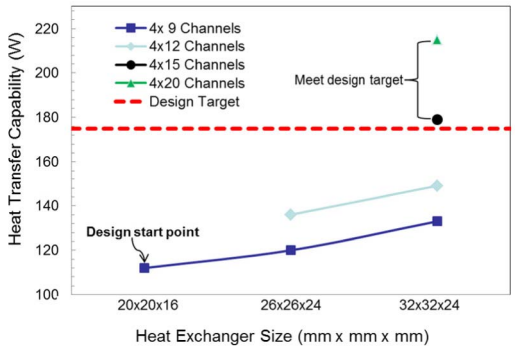

Fig. 13. Variation of the heat transfer capability with the channel numbers and footprint size of Hex-B at the specified conditions.

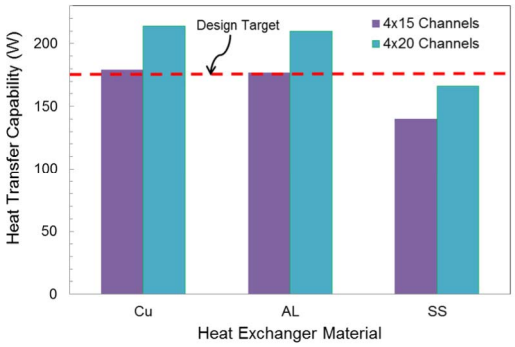

Fig. 14. Effect of the material on the heat transfer capability of Hex-B at the specified conditions.

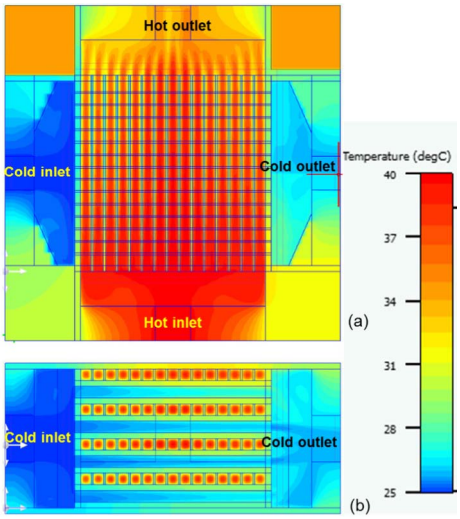

Fig. 15. Simulation results of temperature profile for Hex-B with the final design at the specified condition. (a) Top plane view. (b) Side plane view.

cold flow loop and 40 °C for the hot flow loop. From Fig. 12, it can be found that the heat transfer density is sensitive to flow rate when the flow rate is low (e.g., less than 1 L/min), while it is less sensitive to the flow rate when the flow rate is high (e.g., more than 1 L/min). Besides the heat transfer density, the pressure drop in the heat exchanger, especially in the hot side loop where the mini pump is included, is also important to the cooling system. Lower pressure drop is preferable in practice to lower the pump power. The variation of the pressure drop with the flow rate for Hex-A is also shown in Fig. 12. In this case, the flow rates in the hot flow loop and cold flow loop remain the same. As expected, the pressure drop in the heat exchanger increases with an increase in the flow rate.

To design the compact Hex-B, the simulation model is first built with 4×9 channels in each fluid side with a footprint size of 20 mm $\times$ 20 mm as the design start point. The 6×6 cells are assigned in each channel cross section to ensure the computational accuracy, and the grid independent solution is obtained with a mesh number of 1.2 million. The simulation results are shown in Fig. 13, which presents the heat transfer capability of the Hex-B with different channel numbers and footprint size at the specific conditions. It can be seen that the heat exchanger B with initial configuration (i.e., at the design start point) only provides about 110 W heat transfer capability under the above specified conditions, which is too low for system design target. Therefore, the design is further optimized to increase the power dissipation capability.

The optimization for Hex-B includes: 1) an increase in channel numbers to enlarge heat transfer area; 2) an increase in the footprint size; and 3) use the material with higher thermal conductivity. Fig. 13 shows the effect of channel numbers and footprint size on thermal performance of the customized Hex-B. It is seen that the thermal performance increases as the channel number and footprint size increase. It is also seen from Fig. 13 that for the heat exchangers with a footprint area of 32 mm $\times$ 32 mm and a channel number of $\geq$15, their heat transfer capability exceeds the design power of 175 W, meeting the design target. The effect of heat exchanger material type is shown in Fig. 14. The SS, with a thermal conductivity of 16 W/mK, would have unfavorable thermal performance below the design target, which is not preferred material for Hex-B in this paper. It can also be seen from Fig. 14 that the aluminum heat exchanger has similar thermal performance as that for the copper heat exchanger. Hence, the aluminum heat exchanger is suggested for practical fabrication due to the light weight.

Based on above analysis, the optimized heat exchanger has a footprint area of 32 mm $\times$ 32 mm with a channel number of 15 in each row for both fluids, and it is made of aluminum. Fig. 15 shows the simulation results of the temperature profile for Hex-B with the final design at the following specified conditions. The flow rate is 0.4 L/min in the hot flow loop

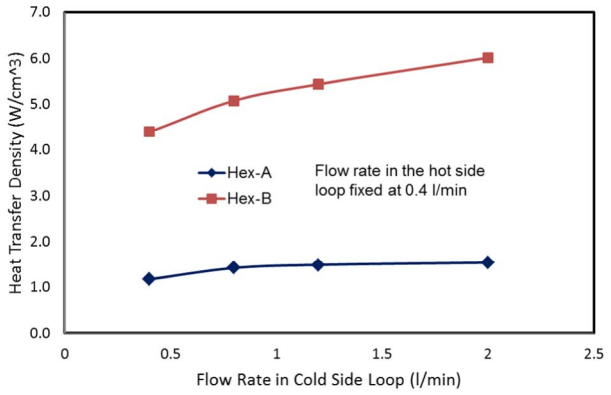

Fig. 16. Comparison of heat transfer density for Hex-A and Hex-B at the specified conditions.

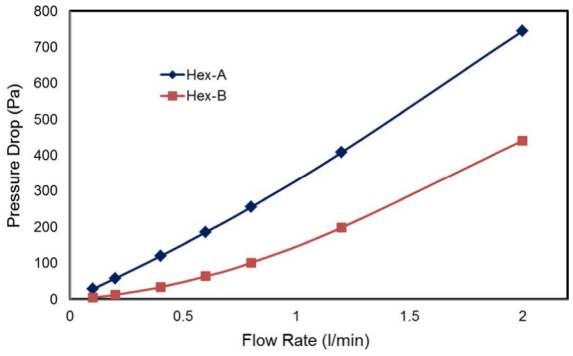

Fig. 17. Comparison of pressure drop for Hex-A and Hex-B at the specified conditions.

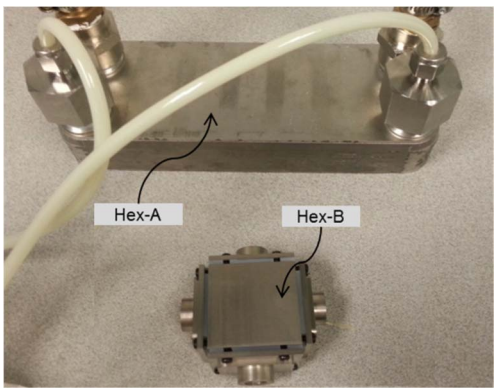

Fig. 18. Comparison of the footprint size between the commercial Hex-A and the customized Hex-B.

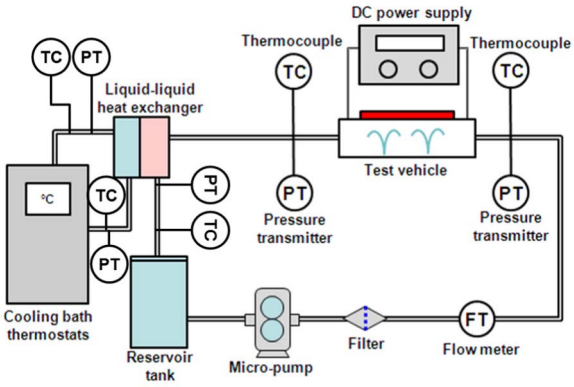

Fig. 19. Schematic of the experimental system.

and 2 L/min in the cold flow loop. The inlet fluid temperature is 25 °C for the cold flow loop and 40 °C for the hot flow loop.

To assess the effectiveness of the design of Hex-B, the heat transfer density, which is defined in the above context, and the pressure drop of Hex-B are compared with those of Hex-A. Fig. 16 presents the comparison of the heat transfer density between commercial Hex-A and customized Hex-B at the specified conditions. Fig. 17 shows the comparison of the pressure drop in Hex-A and Hex-B at the specified conditions. Compared with the commercial heat exchanger (i.e., Hex-A), the much higher heat transfer density and the much lower pressure shown for Hex-B affirm the high effectiveness of this customized compact heat exchanger (i.e., Hex-B).

The optimized Hex-B is fabricated with an aluminum material. It includes dual flow channels for both hot fluid and cold fluid. Silicone rubber was used as sealing ring. In each side, four screws of 4 mm are used to tighten the flange onto the heat transfer core to provide leakage free connection. The overall weight of the newly fabricated heat exchanger is 0.23 kg with all the connecting flanges, which is much less than that for the benchmarking commercial heat exchanger, which weights 1.20 kg. In addition, as indicated in the previous context, the footprint area of the newly fabricated heat exchanger is much smaller than that of the commercial heat exchange, as shown in Fig. 18, which shows the heat exchangers investigated in this paper for the optimized compact heat exchanger (Hex-B) and a comparison of the footprint area between the commercial heat exchanger (Hex-A) and (Hex-B). In addition, Hex-B is with an area ratio of 488 m^2/m^3, that is much larger than that for Hex-A, which is 354 m^2/m^3. Hence, the optimized compact Hex-B has larger heat transfer area ratio and effectiveness. A dedicated leakage test has been conducted for the newly fabricated compact Hex-B, and no leakage is observed at a high gauge pressure of 1 bar.

III. System Assembly and Experiment

An experimental setup is established to evaluate the hydraulic and thermal performance of the proposed liquid cooling system. Prior to the setup of the experimental system, the microcooler test vehicle is first assembled in the following way: the bottom side of the microcooler is attached on the PCB using epoxy, and the thermal test chip on the top surface of the microcooler is wire bonded to the PCB for electrical connection. Fig. 19 shows the schematic of the experimental system, and Fig. 20 shows the photo of the major experimental apparatus for infrared (IR) camera for chip temperature measurement, assembled microcooler test vehicle, commercial heat exchanger (Hex-A) in the flow loop, and alternative compact heat exchanger (Hex-B) in the flow loop.

In the experimental system, a variable-speed microgear pump is used to drive the cooling water from a reservoir tank toward the flow loop. A filter with a 15 μm mesh filter element is used (after the pump) to remove particles

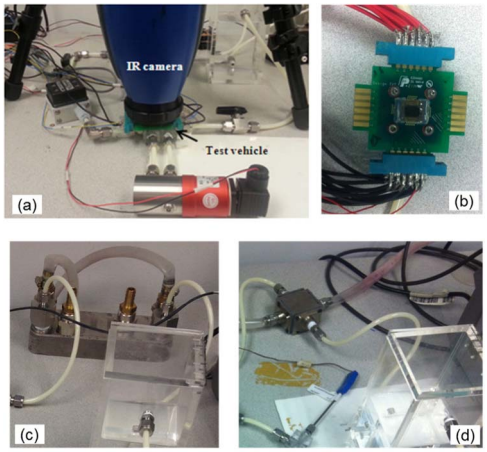

Fig. 20. Photo of the experimental apparatus for (a) IR camera for chip temperature measurement, (b) assembled microcooler test vehicle, (c) Hex-A in the flow loop, and (d) alternative Hex-B in the flow loop.

suspended in the water. The pump forces the water through the filter and a flow meter before it enters the microcooler. The water at the inlet of the microcooler and ambient temperatures is around 25 °C. The differential pressure transducers are attached to a system to measure the pressure drop. The test chip temperature at steady state is measured and recorded using the IR camera. In the experimental test, the steady state (temperature variation ±0.1 °C) is usually reached within 30 min.

First, leakage testing is conducted by running the system at the maximum pressure condition (flow rate is 600 mL/min) for about 6 h. No leakage is observed during this period, which indicates the present bonding and sealing technique for microcooler, and system assembly is working well. Then, the pressure drops of the microcooler, the commercial Hex-A, and the customized Hex-B are measured. Consequently, the dc power is applied to the thermal test chip; the power and chip temperature is measured and recorded to evaluate the thermal performance of the cooling system.

IV. Results and Discussion

In general, besides to improve the thermal performance of the liquid cooling system, another major objective of the design of the liquid cooling system is to reduce the system pressure drop so as to achieve the compactness of the system by selecting the micropump with low pumping power and small size. As previously mentioned, by neglecting the minor pressure drop of fitting and piping, the system pressure drop is the sum of the pressure drop from the microcooler and the heat exchanger. It is important to minimize the pressure drops in the heat exchanger to reduce the overall system pressure drop, since the high pressure drop in the carrier is inevitable due to the requirement of high thermal performance. Without a careful design, the pressure losses from the heat exchanger may be a significant proportion to the system pressure drop.

The variation of the simulated and measured pressure drops versus the flow rate in the heat exchangers and microcooler is presented in Figs. 21 and 22, respectively. It is seen from Figs. 21 and 22 that in the heat exchangers and microcooler considered in this cooling system, the experimentally

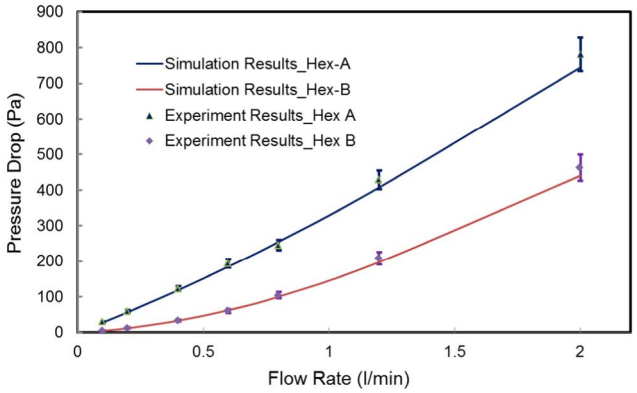

Fig. 21. Pressure drop in commercial heat exchanger (Hex-A) and customized compact heat exchanger (Hex-B).

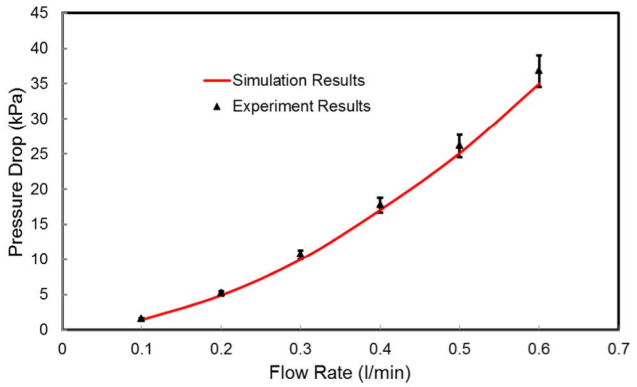

Fig. 22. Pressure drop in microcooler.

measured pressure drop agrees reasonably well with the simulated value, and the simulated results are slightly lower (5%∼10%) than the measured values. The lower pressure drop in the simulation can be attributed to neglecting some small steps between the parts and the rough surface in the flow paths. Taking a closer examination at Figs. 21 and 22, it can be found that the pressure drop in the newly designed and fabricated compact Hex-B is about half of the pressure drop in the commercial Hex-A. It can also be seen that the microcooler with microjet nozzle and microchannels is the main contributor to the pressure drop of the full system, accounting for around 97%∼99% of the system pressure drop, while the heat exchanger only account for about 1%∼3% of the system pressure drop. The proportions of system pressure drop in the microcooler and heat exchanger are shown in Fig. 23. Such a distribution of the system pressure drop indicates that the hydraulic design of this system is efficient, and the pressure drop in the heat exchanger has been reduced to a reasonable level.

The thermal resistance is extracted to evaluate the thermal performance of the full system. The schematic 1-D thermal network of the system is shown in Fig. 24. It is seen that the junction to ambient thermal resistance of the system (θ_{ja}) consists of two parts; the first part is the thermal resistance from the junction to microcooler (θ_{jc}), which represents the thermal performance of the microcooler and the other is the thermal resistance from the microcooler to the ambient (θ_{ca}), which represents the thermal performance of the heat exchanger.

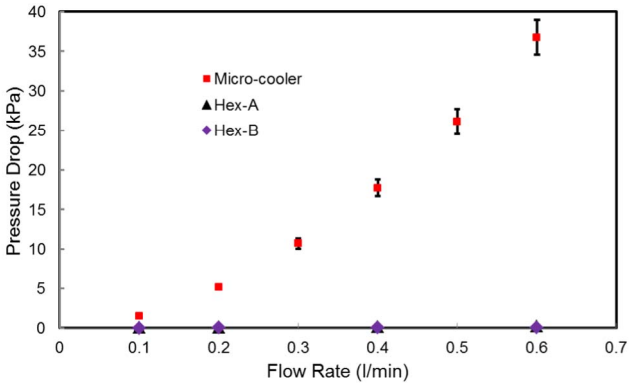

Fig. 23. Comparison of the measured pressure drop in microcooler and heat exchangers.

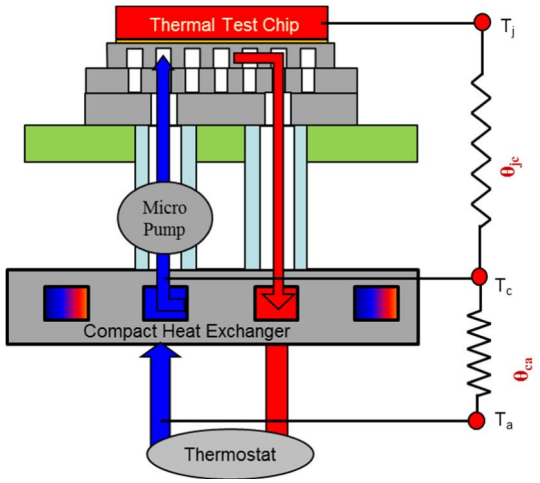

Fig. 24. Schematic of the system thermal resistance analysis.

They are defined by the following equations:

$$\theta_{\mathrm{ja}} = \theta_{\mathrm{jc}} + \theta_{\mathrm{ca}} \tag{2a}$$

$$\theta_{\mathrm{jc}} = (T_j - T_c)/P \tag{2b}$$

$$\theta_{\mathrm{jc}} = (T_c - T_a)/P \tag{2c}$$

where T_j is the junction temperature of the thermal chip and T_c is the cold plate temperature of the microcooler, which refers to the inlet fluid temperature of the microcooler or the outlet fluid temperature in the hot side loop of the heat exchanger in this paper. T_a is the ambient temperature and refer to the thermal bath temperature in this paper.

As mentioned in the context, the design target for this silicon microcooler system is to have a heat dissipation capability of 350 W/cm^2, which corresponds to a heat power of 175 W on a 7 mm × 7 mm chip. Assume the system works in an environment of 40 °C, and the allowable junction temperature is 85 °C. The design target of the junction to ambient thermal resistance for this system is about 0.25 °C/W.

In the tests, the power applied to the thermal test chip varies from 50 to 200 W. The chip temperature under different chip powers is measured, and the results are shown in Fig. 25. The flow rate remains 0.4 L/min in the hot loop and 2 L/min in the cool loop during the test. It can be seen that the chip temperature linearly increases with the increase in the power

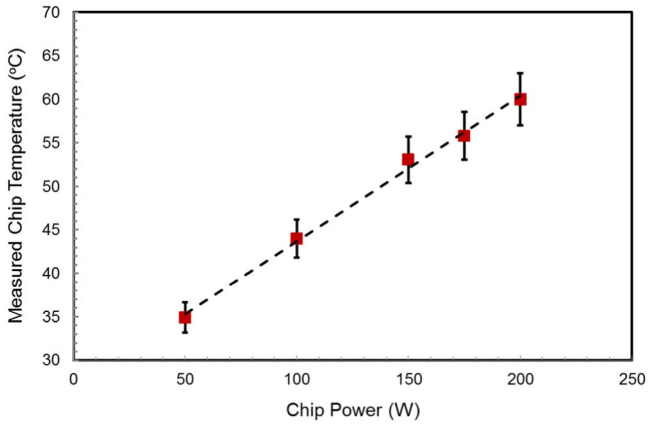

Fig. 25. Measured chip temperature through the IR camera for different chip powers.

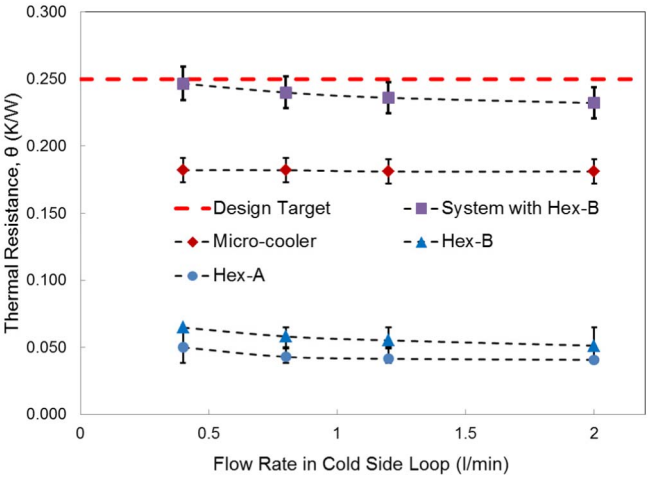

Fig. 26. Measured thermal resistance of the heat exchangers, microcooler, and the full system assembled with compact Hex-B (a power of 175 W).

applied to the chip, while, the overall thermal resistance of the system, including the thermal resistance of the microcooler and the thermal resistance of the heat exchanger, has been obtained. The results are shown in Fig. 26. It can be seen that as the flow rate in the hot flow loop fixes to 0.4 L/min, the variation of the microcooler thermal resistance with the flow rate in the cold flow loop is negligible. However, the thermal resistance of the heat exchangers decreases when the flow rate in the cool flow loop increases, as such causing the decrease in the overall system thermal resistance with the increase of the flow rate in the cold flow loop. Taking a close examination to Fig. 26, it can be found that the microcooler is the main contributor to the overall system thermal resistance, accounting for around 80%∼90% of the total thermal resistance, while the heat exchanger only account for about 10%∼20% of the overall system thermal resistance. In addition, it can be seen that the thermal resistance of the customized Hex-B is slightly larger than that for the commercial Hex-A. While as mentioned in the previous context, Hex-B is much smaller and lighter than Hex-A. Furthermore, the pressure drop in Hex-B is only half of the pressure drop in Hex-A. Furthermore, as shown in Fig. 27, which presents the measured heat transfer density

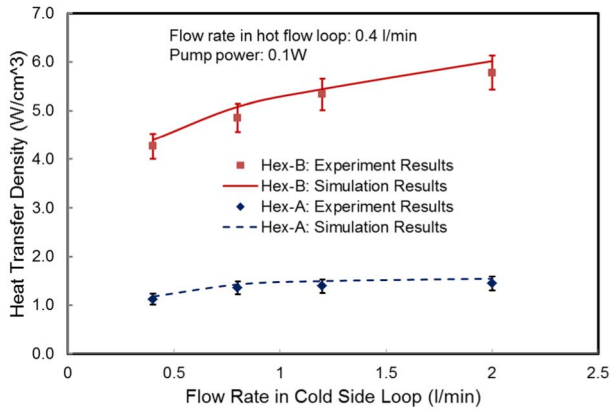

Fig. 27. Measured thermal transfer density for commercial heat transfer A and compact Hex-B (a power of 175 W).

for Hex-A and Hex-B, the heat transfer density of Hex-B is much higher than that for Hex-A. Hence, it can be concluded that the design of Hex-B is more effective than the design of the commercial Hex-A for the applications in this paper. Furthermore, the developed compact cooling system is able to meet the design target of 175-W heat dissipation capability with a pumping power of 0.1 W.

V. Conclusion

A compact and efficient single-phase liquid cooling system is built and examined in this paper. Two major components are developed for the proposed liquid cooling system, including: 1) a silicon-based hybrid microcooler, combining the merits of both microjet array impingement and microchannel flow cooling technologies and 2) a customized compact liquid-to-liquid heat exchanger. The optimized microcooler and the compact heat exchanger have been designed and fabricated. In line with the design and analysis, the experiments for characterizing the flow and heat transfer of the cooling system have been conducted. The pressure drop of the developed major components in the system has been measured. The thermal performance of the liquid cooling system has been evaluated. Some important results are summarized and highlighted as follows.

1) No leakage is observed at a high flow rate of 0.6 L/min (operation flow rate is 0.4 L/min) for the developed cooling system, indicating the present bonding and sealing technique in this cooling system working well.
2) The pressure drop in the heat exchanger is only about 1%∼3% of the total system pressure drop. The thermal resistance of the heat exchanger is only about 10%∼20% of the overall thermal resistance of the system. Such a reasonable level of the pressure drop and thermal resistance for the heat exchanger indicates that the hydraulic and thermal design of this system is efficient to reduce the burden for the microcooler design and the cost for the developed cooling system assembly.
3) The pressure drop in the customized Hex-B is only about 50% of the pressure drop in the commercial Hex-A. The thermal resistance of heat exchange B is slightly larger than that of Hex-A. However, Hex-B, which is with a footprint size of 32 mm × 32 mm and a weight of 0.23 kg, is much smaller (<10% of the footprint area) and lighter (<20% of the mass) than Hex-A, which is with a footprint size of 204 mm × 74 mm and a weight of 1.23 kg, as well the higher thermal transfer density of Hex-B, which is about four times of that for Hex-A, suggesting the effectiveness of the design of the compact Hex-B in this paper.
4) The developed single-phase liquid cooling system has been experimentally demonstrated the heat dissipation capability of 175 W, corresponding to heat density of 350 W/cm^2 on a 7 mm×7 mm chip, with a low pumping power of 0.1 W, meeting the design target of the system.

References

[1] Y. Madhour, S. Zimmermann, J. Olivier, J. Thome, B. Michel, and D. Poulikakos, "Cooling of next generation computer chips: Parametric study for single- and two-phase cooling," in *Proc. 17th Int. Workshop THERMINIC*, Sep. 2011, pp. 1–7.
[2] Y. Mizuno, I. Soga, S. Hirose, O. Tsuboi, and T. Iwai, "Si microchannel cooler integrated with high power amplifiers for base station of mobile communication systems," in *Proc. IEEE 61st ECTC*, May/Jun. 2011, pp. 1541–1546.
[3] S. C. Mohapatra and D. Loikits, "Advances in liquid coolant technologies for electronics cooling," in *Proc. 21st Annu. IEEE Semiconductor Thermal Meas. Manage. Symp.*, Mar. 2005, pp. 354–360.
[4] X. Wei and Y. Joshi, "Stacked microchannel heat sinks for liquid cooling of microelectronic components," *J. Electron. Packag.*, vol. 126, no. 1, pp. 60–66, 2004.
[5] A. Suszko, "Enhancement of nucleate boiling on rough and dimpled surfaces with application to composite spreaders for microprocessors immersion cooling," Ph.D. dissertation, Dept. Mech. Eng., Univ. New Mexico, Albuquerque, NM, USA, Jul. 2015.
[6] J. B. Marcinichen, J. A. Olivier, and J. R. Thome, "On-chip two-phase cooling of datacenters: Cooling system and energy recovery evaluation," *Appl. Thermal Eng.*, vol. 41, pp. 36–51, Aug. 2012.
[7] J. F. Tullius, R. Vajtai, and Y. Bayazitoglu, "A review of cooling in microchannels," *Heat Transf. Eng.*, vol. 21, nos. 7–8, pp. 527–541, 2011.
[8] H. Y. Zhang, D. Pinjala, T. N. Wong, and Y. K. Joshi, "Development of liquid cooling techniques for flip chip ball grid array packages with high heat flux dissipations," *IEEE Trans. Compon. Packag. Technol.*, vol. 28, no. 1, pp. 127–135, Mar. 2005.
[9] H. Bostanci, D. Van Ee, B. A. Saarloos, D. P. Rini, and L. C. Chow, "Thermal management of power inverter modules at high fluxes via two-phase spray cooling," *IEEE Trans. Compon., Packag., Manuf. Technol.*, vol. 2, no. 9, pp. 1480–1485, Sep. 2012.
[10] J. Lee and I. Mudawar, "Low-temperature two-phase microchannel cooling for high-heat-flux thermal management of defense electronics," *IEEE Trans. Compon. Packag. Technol.*, vol. 32, no. 2, pp. 453–465, Jun. 2009.
[11] T. Chen and S. V. Garimella, "Flow boiling heat transfer to a dielectric coolant in a microchannel heat sink," *IEEE Trans. Compon. Packag. Technol.*, vol. 30, no. 1, pp. 24–31, Mar. 2007.
[12] G. Upadhya, M. Munch, P. Zhou, J. Hom, D. Werner, and M. McMaster, "Micro-scale liquid cooling system for high heat flux processor cooling applications," in *Proc. 22nd Annu. IEEE Semiconductor Thermal Meas. Manage. Symp.*, Mar. 2006, pp. 116–119.
[13] Y. Madhour B. P. d'Entremont, J. B. Marcinichen, B. Michel, and J. R. Thome, "Modeling of two-phase evaporative heat transfer in three-dimensional multicavity high performance microprocessor chip stacks," *J. Electron. Packag.*, vol. 136, no. 2, p. 021006, Apr. 2014.
[14] F. Alfieri, M. K. Tiwari, I. Zinovik, D. Poulikakos, T. Brunschwiler, and B. Michel, "3D integrated water cooling of a composite multilayer stack of chips," *J. Heat Transf.*, vol. 132, no. 12, pp. 121402-1–121402-9, Sep. 2010.
[15] M. K. Sung and I. Mudawar, "Single-phase hybrid micro-channel/micro-jet impingement cooling," *Int. J. Heat Mass Transf.*, vol. 51, nos. 17–18, pp. 4342–4352, Aug. 2008.
[16] X. Song *et al.*, "Surrogate-based analysis and optimization for the design of heat sinks with jet impingement," *IEEE Trans. Compon., Packag., Manuf. Technol.*, vol. 4, no. 3, pp. 429–437, Mar. 2014.

[17] M. Fabbri and V. K. Dhir, "Optimized heat transfer for high power electronic cooling using arrays of microjets," *J. Heat Transf.*, vol. 127, no. 7, pp. 760–769, Nov. 2004.
[18] A. J. Robinson, "A thermal–hydraulic comparison of liquid microchannel and impinging liquid jet array heat sinks for high-power electronics cooling," *IEEE Trans. Compon. Packag. Technol.*, vol. 32, no. 2, pp. 347–357, Jun. 2009.
[19] S. Brunschwiler *et al.*, "Direct liquid jet-impingment cooling with micron-sized nozzle array and distributed return architecture," in *Proc. 10th Intersoc. Conf. Thermal Thermomech. Phenomena Electron. Syst. (ITHERM)*, San Diego, CA, USA, May/Jun. 2006, pp. 196–203.
[20] J. Li and G. P. Peterson, "Geometric optimization of a micro heat sink with liquid flow," *IEEE Trans. Compon. Packag. Technol.*, vol. 29, no. 1, pp. 145–154, Mar. 2006.
[21] E. G. Colgan *et al.*, "A practical implementation of silicon microchannel coolers for high power chips," *IEEE Trans. Compon. Packag. Technol.*, vol. 30, no. 2, pp. 218–225, Jun. 2007.
[22] Y. Han, B. L. Lau, H. Zhang, and X. Zhang, "Package-level Si-based micro-jet impingement cooling solution with multiple drainage microtrenches," in *Proc. 16th IEEE EPTC*, Dec. 2014, pp. 330–334.
[23] M. K. Sung and I. Mudawar, "Effects of jet pattern on single-phase cooling performance of hybrid micro-channel/micro-circular-jet-impingement thermal management scheme," *Int. J. Heat Mass Transf.*, vol. 51, nos. 19–20, pp. 4614–4627, 2008.
[24] L. Luo, Y. Fan, W. Zhang, X. Yuan, and N. Midoux, "Integration of constructal distributors to a mini crossflow heat exchanger and their assembly configuration optimization," *Chem. Eng. Sci.*, vol. 62, no. 13, pp. 3605–3619, Jul. 2007.
[25] A. Lozano, F. Barreras, N. Fueyo, and S. Santodomingo, "The flow in an oil/water plate heat exchanger for the automotive industry," *Appl. Thermal Eng.*, vol. 28, no. 10, pp. 1109–1117, Jul. 2008.
[26] H. Y. Zhang *et al.*, "Design considerations on the external heat exchanger for cooling of microelectronic devices," in *Proc. 16th IEEE EPTC*, Dec. 2014, pp. 349–354.
[27] B. L. Lau, Y. L. Lee, Y. C. Leong, K. F. Choo, X. Zhang, and P. K. Chan, "Development of thermal test chip for GaN-on-Si device hotspot characterization," in *Proc. 14th IEEE EPTC*, Dec. 2012, pp. 746–751.

Gongyue Tang received the B.E. degree in mechanical engineering from the Beijing University of Aeronautics and Astronautics, Beijing, China, the M.E. degree in spacecraft design from the Chinese Academy of Space Technology, Beijing, and the Ph.D. degree in mechanical engineering from Nanyang Technological University, Singapore.

He served as a Mechanical Analyst Team Leader with Dyson Operations Pte. Ltd., Singapore, and a Principal Engineer with the United Test and Assembly Center, Ltd., Singapore. He is currently a Research Scientist with the Institute of Microelectronics, a research institute of the Science and Engineering Research Council of the Agency for Science, Technology and Research, Singapore. His current research interests include heat transfer, microfluidics, thermal management, and advanced cooling technologies for integrated circuit packages and microelectronics systems.

Yong Han received the B.S. degree in electronic and information engineering from Shanxi University, Taiyuan, China, in 2004, and the Ph.D. degree in electronic science and technology from the Institute of Electronics, Chinese Academy of Sciences (IECAS), Beijing, China, in 2009.

He was an Assistant Researcher with the Key Laboratory of High Power Microwave Sources and Technologies, IECAS. From 2011 to 2012, he was a Research Associate with the Institute for Research in Electronics and Applied Physics, University of Maryland, College Park, MD, USA. Since 2012, he has been a Research Scientist with the Institute of Microelectronics, Agency for Science, Technology and Research, Singapore. His current research interests include the thermal management of the high power electronic devices, electromagnetic design of the microwave source, computational modeling and thermal analysis, advanced microelectric system packaging development, and electric cooling solutions.

Boon Long Lau received the B.S. degree from the National University of Singapore, Singapore, in 2005.

He was with STMicroelectronics, Geneva, Switzerland, where he was involved in process engineering. Since 2012, he has been with the Institute of Microelectronics, Agency for Science, Technology and Research, Singapore. His current research interests include microchannel and through-silicon-via process integration.

Xiaowu Zhang (SM'10) received the B.S. degree in physics from the National University of Defense Technology, Changsha, China, in 1986, the M.E. degree in mechanics from the University of Science and Technology of China, Hefei, China, in 1989, and the Ph.D. degree in mechanical engineering from the Hong Kong University of Science and Technology, Hong Kong, in 1999.

He was a Lecturer with the Ballistic Research Laboratory of China, East China Institute of Technology, Nanjing, China, from 1989 to 1995. He has been with the Institute of Microelectronics (IME), Agency for Science, Technology and Research, Singapore, since 1999, where he is currently a Principal Investigator with the Interconnection and Advanced Packaging Program. He has authored or co-authored over 120 technical papers in refereed journals and conference proceedings. His current research interests include computational modeling and stress analysis, design for reliability, stress sensors, impact dynamics, advanced integrated circuit (IC) and microsystems packaging development, and 3-D IC integration with through-silicon-via technology.

Daniel Min Woo Rhee was born in Seoul, South Korea, in 1973. He received the B.Eng., M.S., and Ph.D. degrees from Sogang University, Seoul, in 1996, 1998, and 2010, respectively, all in chemical engineering.

He has been involved in microelectronics packaging research and development for both the industry and the research institute for more than 15 years and has extensive experience in new packaging and material development, numerical modeling, and characterization. At the Institute of Microelectronics (IME), Agency for Science, Technology and Research, Singapore, he is currently leading power module and ruggedized electronics group and industry consortium projects for automotive, oil and gas, deep sea exploration, and aerospace industries. has led projects of a lot of public funded and industry projects related to material and new packaging development, such as microelectromechanical systems, 3-D IC packaging, and power electronics packaging solution for SiC/GaN devices since he joined IME in 2011. Before he joined IME, he had developed automotive three phase inverter modules for high power electronics with the Fairchild Semiconductor Research and Development Group, Seoul, as a Principle Engineer which were successfully applied for mass production for automotive industries. He was with Amkor Technology Research and Development as the Senior Manager and Leader of material characterization modeling and failure analysis group and resolved lots of chronicle failure and quality issues with worldwide semiconductor companies from 1999 to 2010. He has authored or co-authored over 60 journal and conference papers and holds about 20 patents in microelectronics materials and packaging fields.

Dr. Rhee received the Best Employee of the Year Award in 2009.